Dispersion Characteristics of the Dipolar Modes in a Waveguide Partially Filled with a Magnetized Ferrite Column

S. LE-NGOC, G. L. YIP, SENIOR MEMBER, IEEE, AND S. NEMOTO

Abstract—**The electromagnetic wave propagation in a partially filled ferrite waveguide is studied by using both the quasi-static and exact analyses. Here, the ferrite is assumed to be lossless and completely magnetized. The cutoff and resonant frequencies are examined analytically to predict all possible modes, and numerical methods are then used to study the complete dispersion characteristics. Because of the geometrical generality of the problem, the fully filled ferrite waveguide and the ferrite column in free space can be considered as special cases. The classifications of the modes existing in various parametric regions are clarified. The effects of the ratio of the ferrite-to-waveguide radius and the dc axial magnetic field on the behaviors of the modes are studied and discussed. For large values of the phase constant, asymptotic dispersion equations can be derived, and turn out to be the same in both analyses. A comparison between the two sets of results is also made to examine the validity of the quasi-static analysis. The method of analysis used in the present paper is similar to the one used in the corresponding paper on partially filled plasma waveguides published previously [1].**

NOTATION

In a cylindrical coordinate system (r,ϕ,z), the fields are assumed:

$F(r,\phi,z)$ $= F(r) \exp [j(kz + n\phi - \omega t)]$
k phase constant;
n azimuthal variation number;
ω operating frequency;
ω_m saturation magnetization frequency;
k_0 free-space phase constant;
c velocity of light in free space;
$\Omega = \omega/\omega_m$ normalized frequency;
$\Omega_H = \omega_H/\omega_m$ normalized gyromagnetic frequency;
$\gamma = k/k_0$ normalized phase constant;
$s_0 = b/a$ ratio of radii (b and a are the radii of ferrite column and waveguide, respectively);
$q = \omega_m b/c$ normalized ferrite column radius;

$$E(r) = \sqrt{\varepsilon_0}\, E_1(r) \quad H(r) = \sqrt{\mu_0}\, H_1(r)$$

where $|E_1(r)$ and $|H_1(r)$ are the normalized field vectors, and ε_0 and μ_0 are the permittivity and permeability of free space, respectively.

$\bar{\mu}$ permeability tensor;
$\bar{\mu} = \mu_1 \hat{r}\hat{r} + j\mu_2 \hat{r}\hat{\phi} + \mu_1 \hat{\phi}\hat{\phi} - j\mu_2 \hat{\phi}\hat{r} + \hat{z}\hat{z}$
$\mu_1 = 1 + \Omega_H/(\Omega_H^2 - \Omega^2)$ $\mu_2 = -\Omega/(\Omega_H^2 - \Omega^2)$
ε_r: relative dielectric constant of the ferrite column;
$J_n(x), N_n(x)$ the Bessel functions of the first and second kind, respectively;
$I_n(x), K_n(x)$ the modified Bessel functions of the first and second kind, respectively.

Manuscript received August 14, 1975; revised August 2, 1976.
The authors are with the Department of Electrical Engineering, McGill University, Montreal, P.Q., Canada.

I. INTRODUCTION

SOME ASPECTS OF electromagnetic wave propagation in fully filled and partially filled ferrite waveguides as well as in ferrite column in free space have been studied theoretically by several authors. The theoretical analyses were mainly based on two approaches: the quasi-static approximation and the exact analysis. In the quasi-static approximation, the RF electric fields are so small that they can be neglected, and therefore, the fields are derived from a scalar potential [2]–[6]. In the exact analysis, the fields are obtained by solving the full Maxwell's equations [7]–[12].

By using the quasi-static approximation, Trivelpiece *et al.* [2] formulated the dispersion equations for the fully filled, partially filled ferrite waveguides, and for the ferrite column in free space. However, only the dispersion relations for the fully filled ferrite waveguide and for the ferrite column in free space were computed for the axisymmetric ($n = 0$) and the dipolar modes ($n = \pm 1$). Joseph and Schlömann [3] solved the dispersion equation for the ferrite column in free space for both cases ($n = 0, \pm 1$), and their results were experimentally verified by Bini *et al.* [4] and by Olson *et al.* [5]. Although Masuda *et al.* [6] examined the partially filled ferrite waveguide problem, their work was restricted to the dipolar surface-wave modes.

With the exact analysis, Kales [7] formulated the dispersion equations for the fully filled and partially filled ferrite waveguides. However, he discussed the cutoff frequencies for the fully filled case only qualitatively, and no numerical results were given. Suhl and Walker [8] considered in detail the fully filled waveguide. Although Tompkins [9] tackled the partially filled ferrite waveguide, his work was restricted to a specific frequency and a weak dc magnetic field. Recently, Duputz and Priou [10] have initiated a computing method to solve the dispersion equations for the fully filled and partially filled waveguides by assuming that the ferrite is lossy. However, their work is restricted to the $TE_{1,1}$ mode at a fixed frequency of 9.5 GHz. The propagation characteristics of the ferrite column in free space were investigated by Schott *et al.* [11] and Tao *et al.* [12], who did not consider cutoffs and resonances.

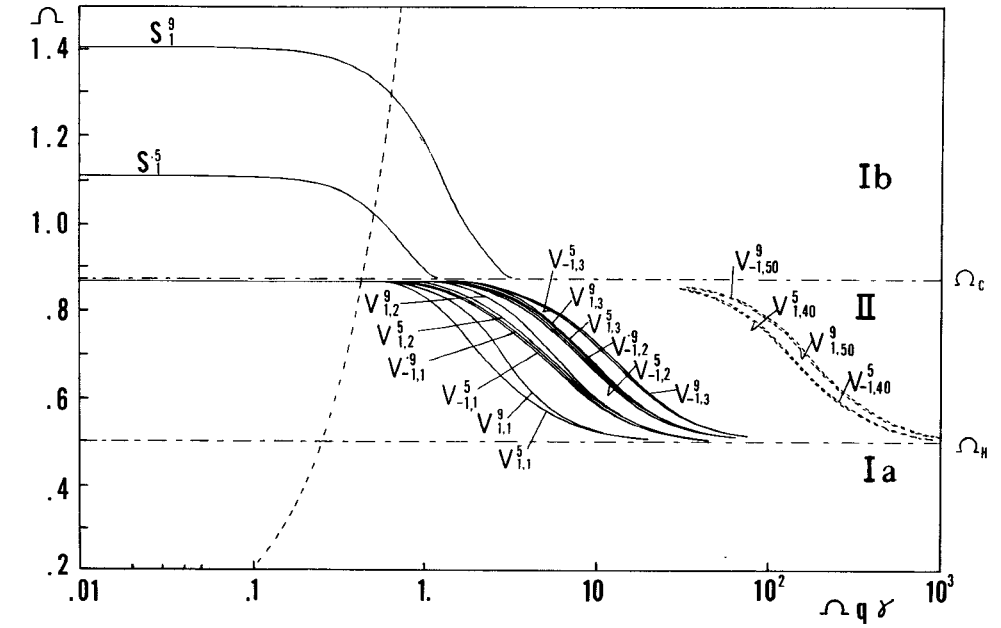

(a)

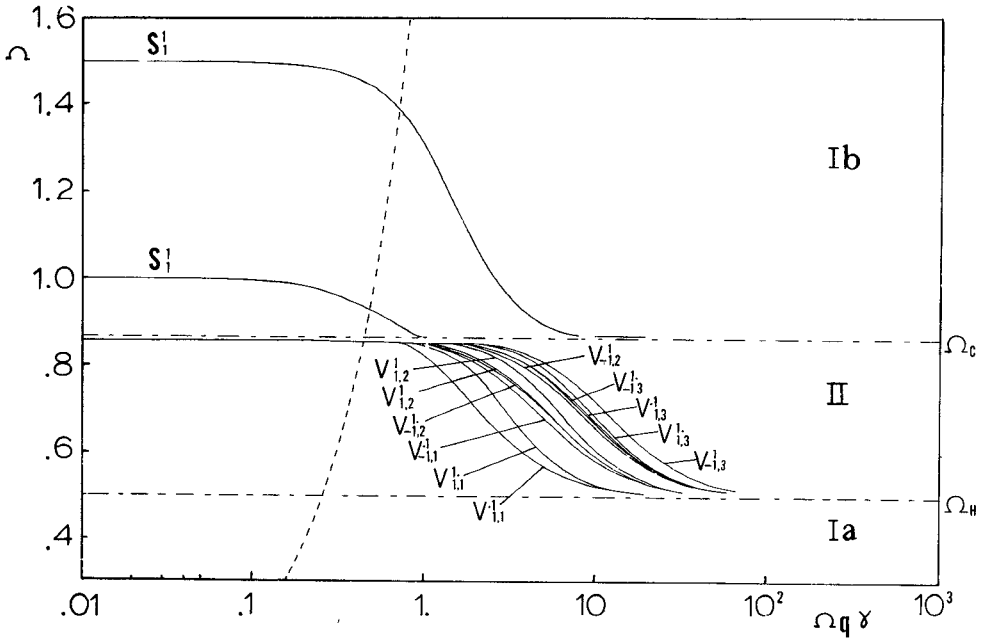

(b)

Fig. 1. (a) Magnetostatic dispersion curves for $n = \pm 1, q = 0.5, \Omega_H = 0.5, s_0 = 0.9, 0.5$. (b) Magnetostatic dispersion curves for $n = \pm 1, q = 0.5, \Omega_H = 0.5, s_0 = 1, 0.1$.

II. The Quasi-Static Dispersion Characteristics

The field solutions are derived on the assumption that the phase velocities of the waves are much less than the velocity of light, so that the RF electric fields can be neglected. The magnetic fields are derived from a scalar function Φ, i.e., $H = \nabla\Phi$. This approximation is, therefore, called magnetostatic approximation. By imposing the boundary conditions ($B_r = 0$ at $r = a$, the continuity of B_r and H_z at $r = b$), the dispersion equations are obtained and given in Appendix I.

A. Cutoffs

The frequencies at which propagation just begins, i.e., $\gamma = 0$, are referred to as the cutoff frequencies. When γ approaches zero, the right-hand side F_n of (A1) is approximated by

$$\lim_{\gamma \to 0} F_n = -(|n|/b)(1 - s_0^{2|n|})/(1 + s_0^{2|n|}). \qquad (1)$$

From (A2), $u^2 < 0$ in regions Ia ($0 < \Omega < \Omega_H$) and Ib ($\Omega > \Omega_c$) in Figs. 1 and 2 and $u^2 > 0$ in region II

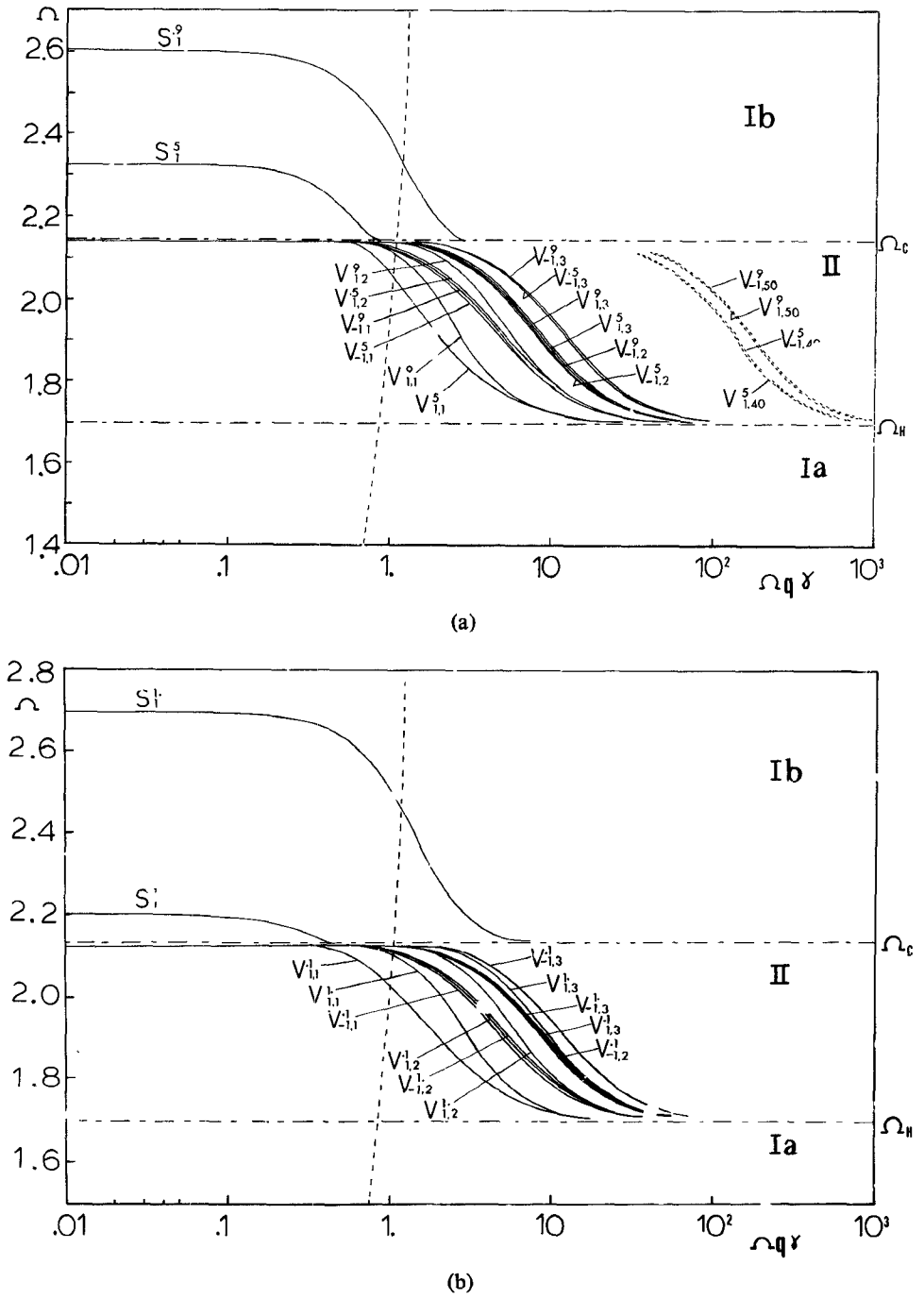

Fig. 2. (a) Magnetostatic dispersion curves for $n = \pm 1$, $q = 0.5$, $\Omega_H = 1.7$, $s_0 = 0.9, 0.5$. (b) Magnetostatic dispersion curves for $n = \pm 1$, $q = 0.5$, $\Omega_H = 1.7$, $s_0 = 1, 0.1$.

($\Omega_H < \Omega < \Omega_c$) where $\Omega_c = |\Omega_H(\Omega_H + 1)|^{1/2}$. In the case $u^2 < 0$, the left-hand side of (A1) can be approximated by

$$\lim_{\gamma \to 0} G_{\pm n} = (|n|/b)(\Omega_H \mp \Omega + 1)/(\Omega_H \mp \Omega) \qquad (2)$$

where the upper (lower) sign corresponds to positive (negative) n. From (1) and (2) only one cutoff frequency is found for positive n:

$$\Omega_s = \Omega_H + \delta(1 + \delta)^{-1} \qquad (3)$$

where $\delta = (1 + s_0^{2|n|})/(1 - s_0^{2|n|})$. When s_0 tends to zero (ferrite column in free space), $\Omega_s = \Omega_H + (1/2)$, and for the fully filled case, $\Omega_s = \Omega_H + 1$. In the case $u^2 > 0$, $G_{\pm n}$ can oscillate from $-\infty$ to $+\infty$ [1]. Hence there will be an infinite number of solutions in region II. From (A2), it can be shown that Ω_c is the common cutoff frequency for all the modes in this region.

B. Resonances

The frequencies at which the phase constant tends to infinity are referred to as the resonant frequencies. When γ

tends to infinity, F_n can be approximated by

$$\lim_{\gamma \to \infty} F_n = -k_0 \gamma < 0. \tag{4}$$

In the case $u^2 < 0$, $G_{\pm n}$ is reduced to

$$\lim_{\gamma \to \infty} G_{\pm n} = k_0 \gamma \mu_1^{1/2} > 0. \tag{5}$$

Therefore, there is no resonant frequency in regions Ia and Ib. However, since $F_n = 0$ for the fully filled case ($S_0 = 1$), there exists a resonant frequency at $\Omega = \Omega_c$. In the case $u^2 > 0$, since $G_{\pm n}$ is oscillatory, there exists an infinite number of roots for (A1). For large values of γ, the dispersion equation (A1) can be simplified by a similar method as used in [1], to

$$\Omega q \gamma_m = \begin{cases} (-\mu_1)^{1/2}[\theta + \pi(m - 0.75)], & n = 1 \\ (-\mu_1)^{1/2}[\theta + \pi(m + 0.25)], & n = -1 \end{cases} \tag{6}$$

where $\tan \theta = (-\mu_1)^{1/2}$, $0 < \theta < \pi/2$, and $m = 1,2,3,\cdots$. The mode order m should be chosen consistently with the mode designation discussed later in Section III. For the fully filled case, we obtain

$$\Omega q \gamma_m = \pi(-\mu_1)^{1/2}(m - 0.25), \qquad n = \pm 1 \tag{7}$$

where $m = 1,2,3,\cdots$. From (6) and (7), the gyromagnetic resonance frequency $\Omega = \Omega_H$ is found as the resonant frequency for all the modes.

C. Numerical Results

A numerical iterative procedure is now used to solve the dispersion equations (A1) and (A2). Throughout this paper, the normalized ferrite column radius is chosen at a fixed value $q = 0.5$, which could, for example, correspond to $b = 1.5$ cm for $\omega_m = 10^{10}$ rad/s. The results are shown in Fig. 1(a) and (b) for a weak dc magnetic field ($\Omega_H = 0.5$) and in Fig. 2(a) and (b) for a strong dc magnetic field ($\Omega_H = 1.7$). The representative ratios of radii $s_0 = 0.9$ and $s_0 = 0.5$ have been chosen for the study of the dispersion characteristics of the partially filled ferrite waveguide. The two limiting cases $s_0 = 1$ (the fully filled ferrite waveguide) and $s_0 = 0.1$ (almost a ferrite column in free space) are also presented in Fig. 1(b) for $\Omega_H = 0.5$ and in Fig. 2(b) for $\Omega_H = 1.7$. In region Ia, cutoffs and resonances are nonexistent and numerical probing has yielded no solutions, leading to the conclusion that no modes exist in this region. According to their cutoffs and their physical characteristics, the various modes can be classified into surface-wave modes and volume modes. The surface-wave modes designated ${}^{\Omega_H}_{q}S_n^{s_0}$ are characterized by the concentration of field energy at the ferrite–air interface, and the volume modes designated ${}^{\Omega_H}_{q}V_{nm}^{s_0}$ are characterized by the predominant distribution of field energy within the volume of the ferrite column. The proposed mode designations are consistent with those for the partially filled plasma waveguide [1].

For relatively weak magnetic fields, it is seen from Fig. 1(a) and (b) that the surface-wave modes are restricted to the region where γ is small. These modes start at the cutoff frequency Ω_s above Ω_c, slope down with decreasing Ω, and terminate at a point on the line $\Omega = \Omega_c$, where its group velocity can be analytically shown to be zero [16]. They are all backward waves and the dependence of Ω_s on s_0 is also seen. The numerical method verifies that the surface-wave modes exist only for positive n as predicted previously. The volume modes are entirely restricted to the slow-wave region on the right of the dotted line. These modes start from $\Omega = \Omega_c$, slope down with decreasing Ω, and asymptotically approach $\Omega = \Omega_H$. They are all backward slow waves. As s_0 increases, they are shifted to the region of larger γ, and near the gyromagnetic resonance, they are almost independent of s_0. For relatively strong magnetic fields, as seen from Fig. 2(a) and (b), the surface-wave and volume modes retain their basic features except that the phase velocities increase and some volume modes pass the light line becoming fast waves. Note that the $V_{-1,1}^{1}$ mode does not exist, i.e., its root cannot be found. The first root ua lies in the second interval of the quotient function. As will be seen later, the $V_{-1,1}^{1}$ does exist in the exact analysis. This discrepancy is due to the fact that the magnetostatic dispersion relation is not strictly valid at small values of γ.

For the higher order volume modes, the asymptotic dispersion equation (6) was used to obtain the dotted curves $V_{\pm 1,40}^{0.5}$ and $V_{\pm 1,50}^{0.9}$ shown in Figs. 1(a) and 2(a). These asymptotic results agree with those computed from the dispersion equations (A1) and (A2). It is observed from Table I that the agreement between the two results can be seen even for the third-order modes. This establishes the validity of the asymptotic dispersion equations. The volume modes can, therefore, be obtained without a numerical iterative procedure in order to save the computing time [1].

TABLE I
RESULTS OF MAGNETOSTATIC ANALYSIS

	Computed Results		Asymptotic Results	
	Ω	$\Omega q \gamma$	Ω	$\Omega q \gamma$
$V_{1,3}^{.5}$	.7	8.27	.7	8.19
	.6	15.42	.6	15.34
$V_{1,40}^{.5}$	.7	129.18	.7	129.18
	.6	234.22	.6	234.21
$V_{-1,3}^{.5}$	.7	11.27	.7	11.46
	.6	20.93	.6	21.26
$V_{-1,40}^{.5}$	.7	132.43	.7	133.26
	.6	240.10	.6	240.13

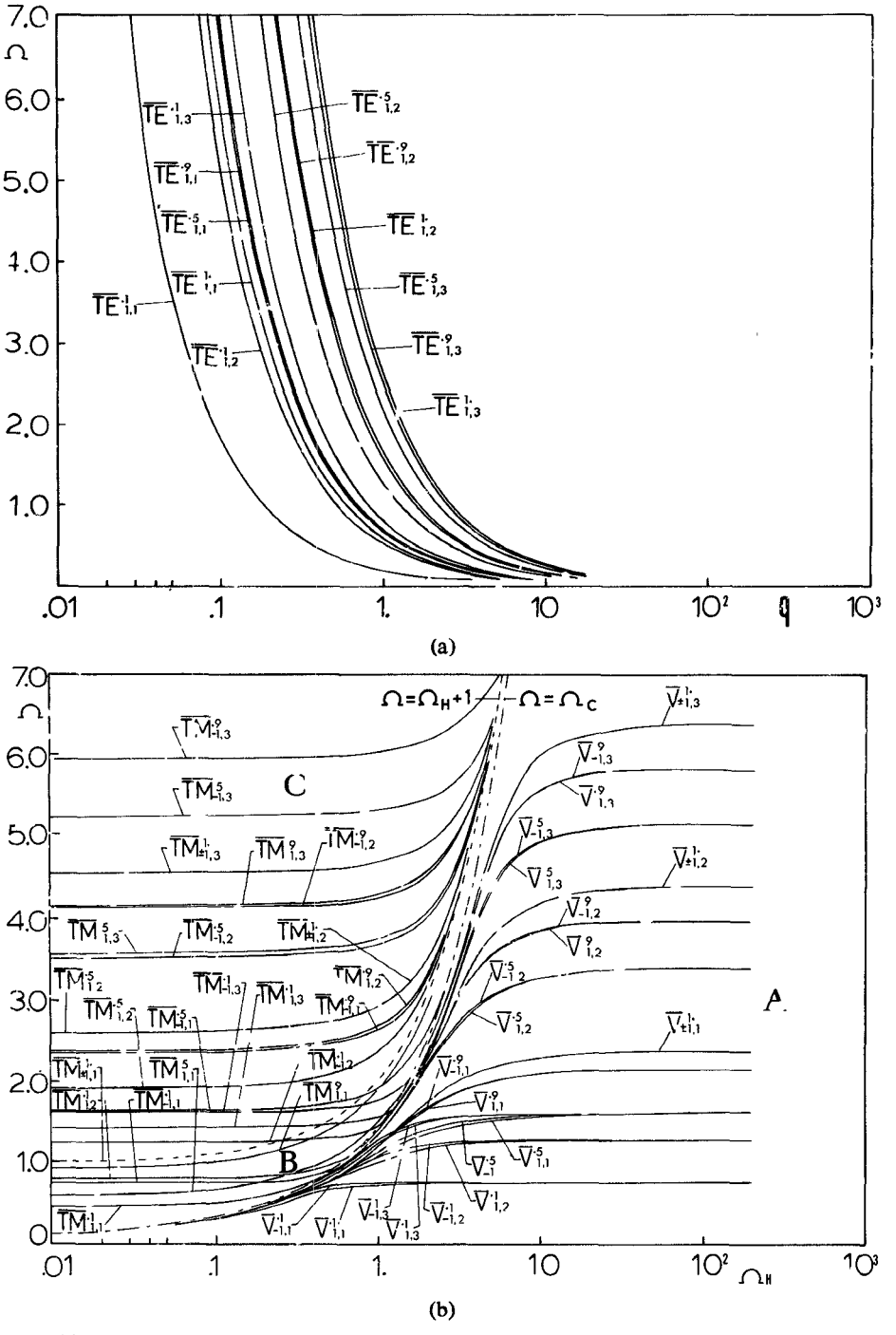

Fig. 3. (a) Cutoff frequencies of transverse electric modes, $n = \pm 1$. (b) Cutoff frequencies of transverse magnetic modes, $n = \pm 1$.

III. Exact Dispersion Characteristics

The exact field solutions are now derived directly from Maxwell's equations. The dispersion equations obtained through the imposition of the boundary conditions ($E_z = 0$, $B_r = 0$ at $r = a$, the continuity of E_z, H_z, B_r, and H_ϕ at $r = b$) are given in Appendix II.

A. Cutoffs

In general, the modes are hybrid in nature. However, at cutoff it can be shown that they are split up into purely transverse electric (TE) modes and purely transverse magnetic (TM) modes [7]. The dispersion equations (A10) and (A11) for the TE modes are independent of Ω_H and the sign of n. The Ω_H independence can be explained by the fact that, at cutoff, the RF magnetic field is parallel to the dc magnetic field H_0, so that the ac magnetic field does not contribute to the motion of the magnetization vector and is, therefore, unaffected by H_0. Equations (A10) and (A11) are numerically solved for several modes, and the solutions are plotted against the normalized ferrite column radius q

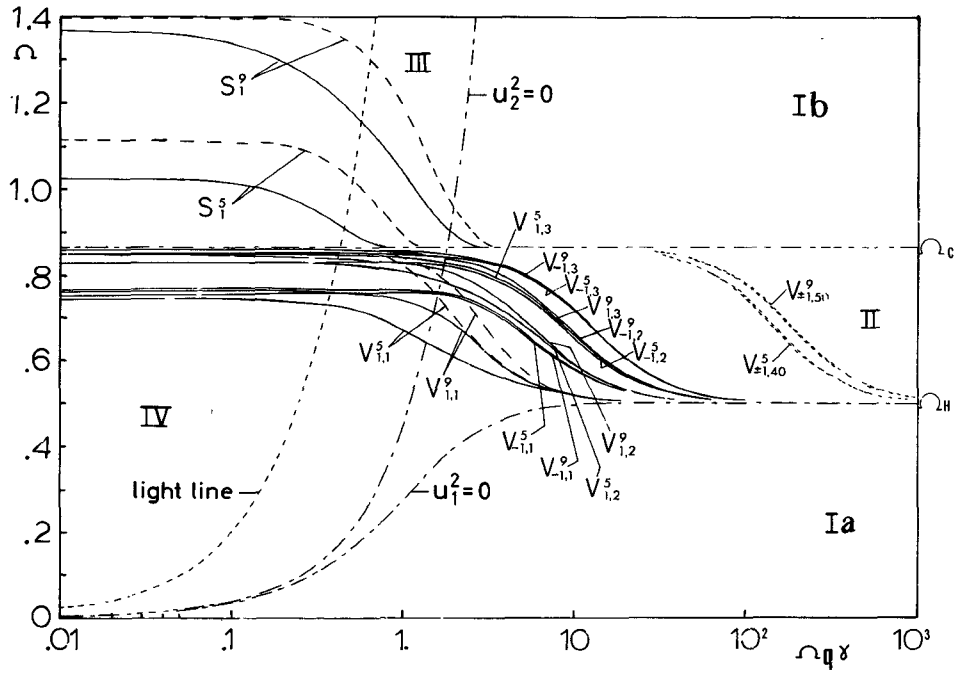

(a)

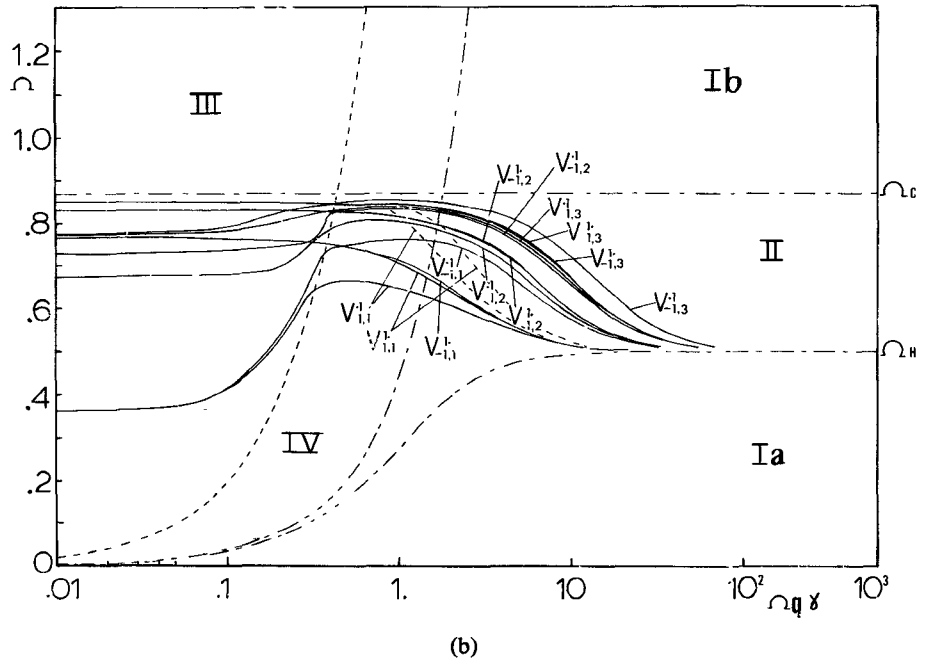

(b)

Fig. 4. (a) Exact dispersion curves for $n = \pm 1$, $q = 0.5$, $\Omega_H = 0.5$, $s_0 = 0.9, 0.5$, $\varepsilon_r = 10$. – – – magnetostatic results. (b) Exact dispersion curves for $n = \pm 1$, $q = 0.5$, $\Omega_H = 0.5$, $s_0 = 1, 0.1$, $\varepsilon_r = 10$. – – – magnetostatic results.

in Fig. 3(a). Each cutoff curve is designated as $\overline{\text{TE}}_{np}^{s_0}$, where p indicates the increasing order of the cutoff frequency curves. For the fully filled waveguides, the dispersion equation at cutoff is obtained by setting $b = a$ in (A10). As q increases, the TE cutoff frequencies decrease rapidly and tend to zero. For a fixed value of q, they increase considerably as s_0 increases.

The dispersion equations (A12) and (A13) for the TM modes depend not only on the sign of n but also on Ω_H, because, at cutoff, the RF magnetic field is transverse to H_0, so that the RF magnetic field contributes to the motion of the magnetization vector and is now affected by H_0. The TM cutoff frequencies are plotted against Ω_H in Fig. 3(b). The dotted curves $\Omega = \Omega_H + 1$ ($u_1^2 = 0$) and $\Omega = \Omega_c$ ($u_1^2 = \infty$) divide the $\Omega - \Omega_H$ plane into three regions: A ($\Omega < \Omega_c$), B ($\Omega_c < \Omega < \Omega_H + 1$), and C ($\Omega > \Omega_H + 1$). U_1 is real in regions A and C, and imaginary in region B.

It is clear that the curve $\Omega = \Omega_c$ separates two groups of modes. One occupying region A determines the cutoff frequencies of the volume modes and are designated as $\overline{V}_{np}^{s_0}$. The others occupying regions B and C determine the cutoff frequencies of the surface-wave modes and the modified

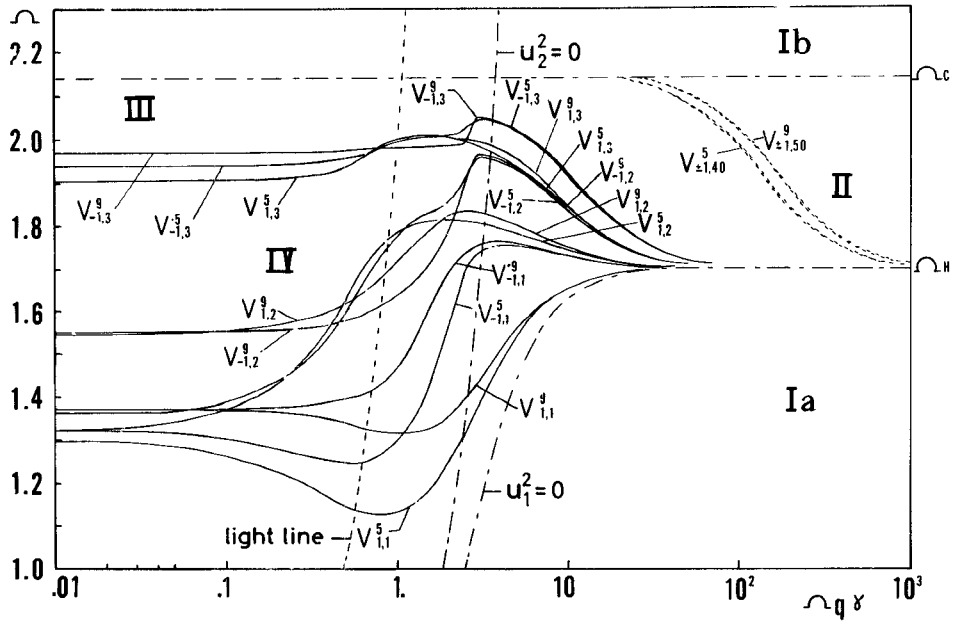

(a)

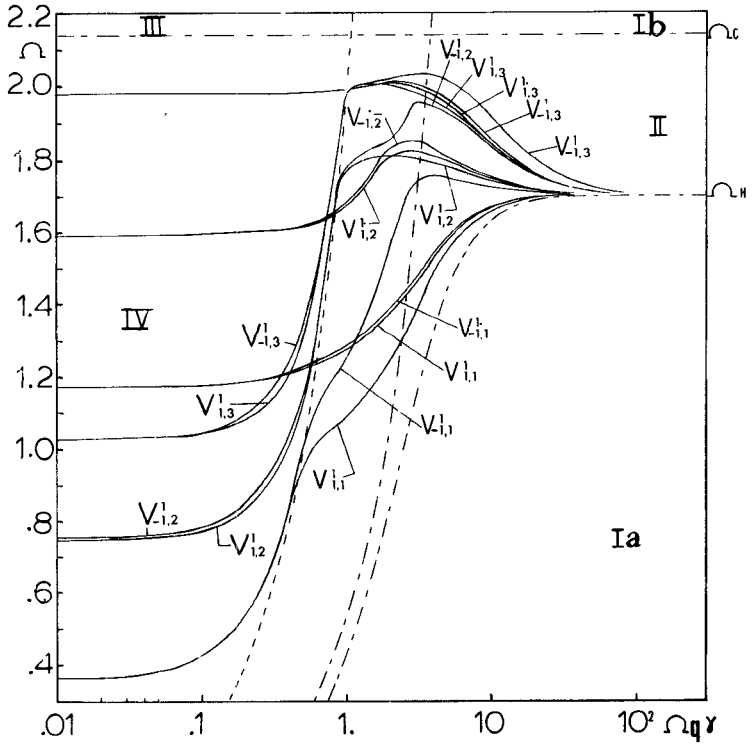

(b)

Fig. 5. (a) Exact dispersion curves for $n = \pm 1$, $q = 0.5$, $\Omega_H = 1.7$, $s_0 = 0.9, 0.5$, $\varepsilon_r = 10$. – – – magnetostatic results. (b) Exact dispersion curves for $n = \pm 1$, $q = 0.5$, $\Omega_H = 1.7$, $s_0 = 1, 0.1$, $\varepsilon_r = 10$.

waveguide modes, and are designated as $\overline{\mathrm{TM}}_{np}^{s_0}$. The cutoff curves $\overline{V}_{np}^{s_0}$ start from Ω_c and increase rapidly along the line $\Omega = \Omega_c$ as Ω_H increases, but when Ω_H is large, they are almost independent of Ω_H. It can be shown analytically that all the cutoff curves designated as $\overline{\mathrm{TM}}_{np}^{s_0}$ are asymptotic to the curve $\Omega = \Omega_c$ in the limit of $\Omega \to \infty$. For the fully filled waveguide, the dispersion equation at cutoff is obtained by setting $b = a$ in (A12), i.e., $J_n(u_1 a) = 0$, which is independent of the sign of n. The lowest order solution of $J_n(u_1 a) = 0$ is $u_1 a = 0$, i.e., $\Omega = \Omega_H + 1$ which forms the boundary curve between regions B and C.

B. Resonances

When γ tends to infinity, the radial wave numbers given in (A4) can be approximated to obtain the magnetostatic results, i.e., ${u_1}^2 = u^2$, ${u_2}^2 = -k^2$. In region I, u_1 is imaginary. Equation (A3) can be analytically solved to prove that there are no resonant frequencies in this region.

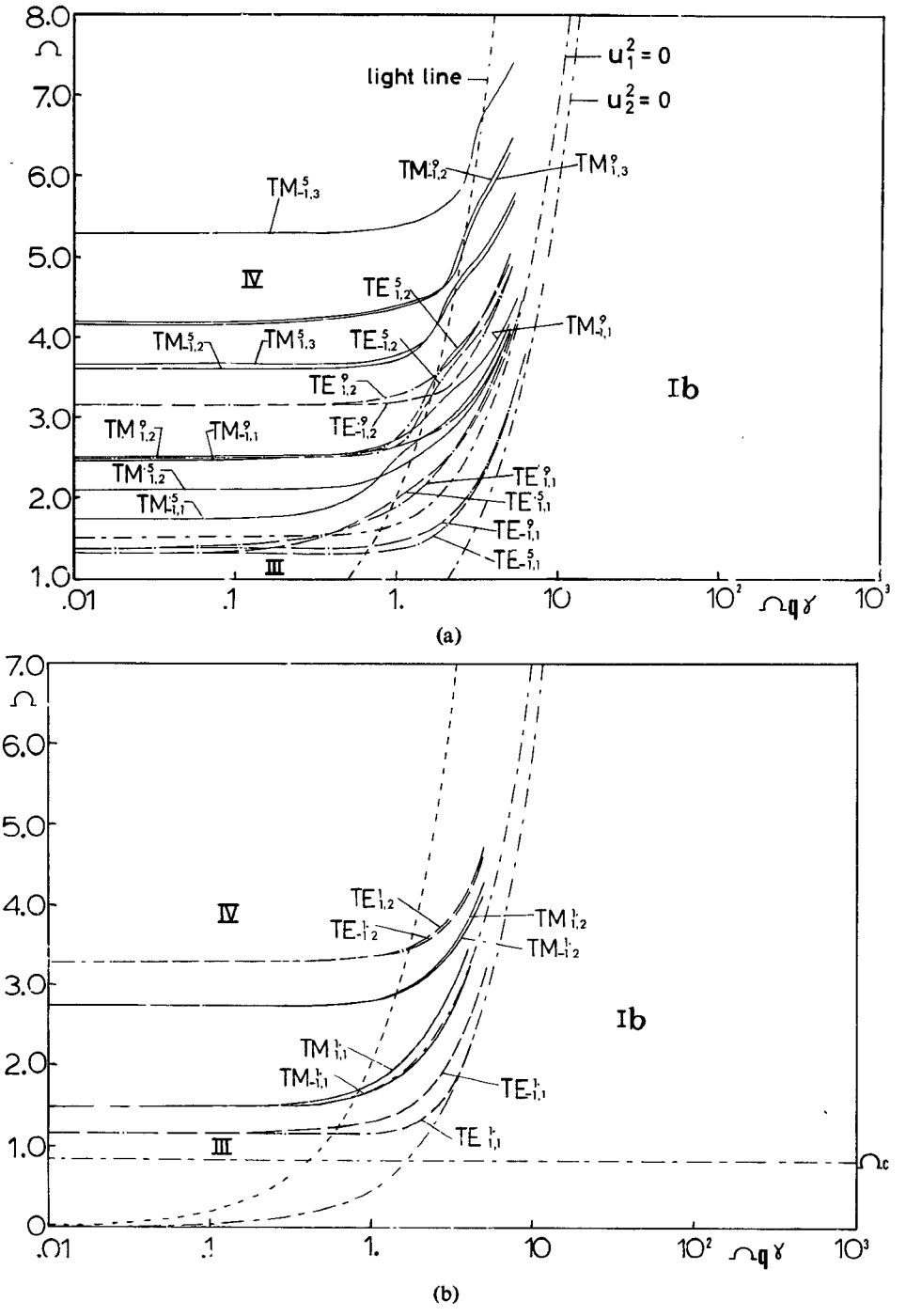

Fig. 6. (a) Modified waveguide modes for $n = \pm 1$, $q = 0.5$, $\Omega_H = 0.5$, $s_0 = 0.9, 0.5$, $\varepsilon_r = 10$. (b) Modified waveguide modes for $n = \pm 1$, $q = 0.5$, $\Omega_H = 0.5$, $s_0 = 1$, $\varepsilon_r = 10$.

In region II, u_1 is real. Equation (A3) can be approximated to yield the same asymptotic dispersion equation (6).

For the fully filled case, the dispersion equation is obtained by letting $a = b$ in (A3) and the asymptotic dispersion equation (7) is again found. Using (6) and (7), the gyromagnetic resonance frequency can again be found.

C. Numerical Results

The values of parameters used for the magnetostatic results are also adopted here, and ε_r is chosen to be 10 as a representative value of dielectric constant of ferrite [13]. The computational part is now much more complicated than the one in the magnetostatic approximation because of the mathematical complexity and the presence of the following four parametric regions: I) where u_1 and u_2 are both imaginary, II) where u_1 is real and u_2 imaginary, III) where u_1 is imaginary and u_2 real, and IV) where u_1 and u_2 are both real. These regions are indicated in Figs. 4–8. Note that when $\gamma \to \infty$ regions I and II correspond to regions I and II, respectively, in the quasi-static analysis.

All the modes existing in the magnetostatic approximation are shown in Fig. 4(a) and (b) for $\Omega_H = 0.5$ and in

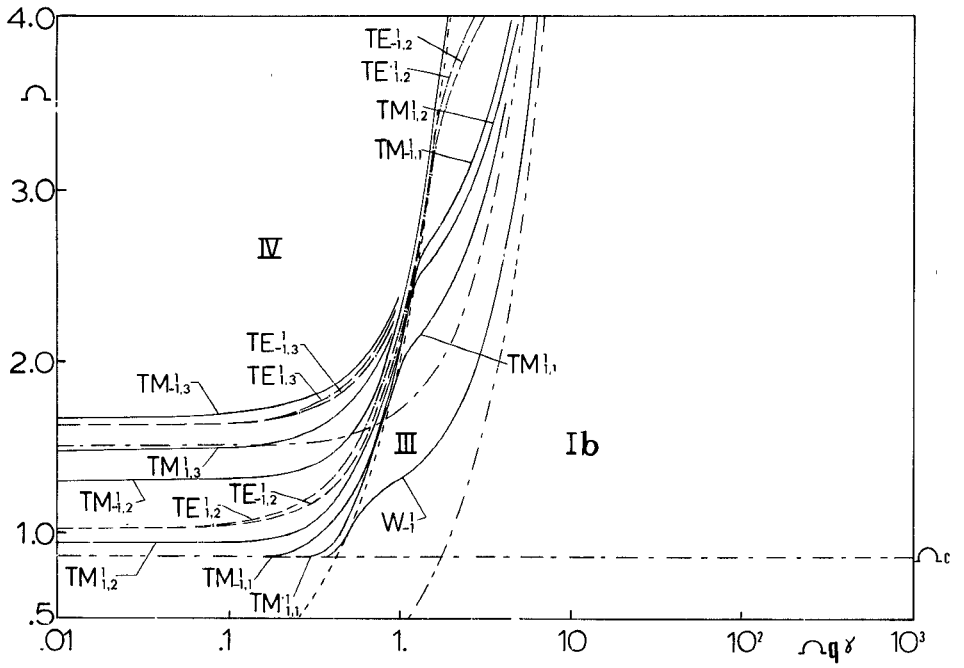

(c)

Fig. 6. (c) Modified waveguide modes for $n = \pm 1$, $q = 0.5$, $\Omega_H = 0.5$, $s_0 = 0.1$, $\varepsilon_r = 10$.

Fig. 5(a) and (b) for $\Omega_H = 1.7$. As defined in Section II-C, these modes are classified into the surface-wave modes, $S_n^{s_0}$, and the volume modes, $V_{nm}^{s_0}$. All the modes which cannot be predicted by the magnetostatic approximation are presented in Fig. 6(a)–(c) for $\Omega_H = 0.5$ and in Fig. 7(a)–(c) for $\Omega_H = 1.7$. They are virtually the modes existing in an isotropic ferrite waveguide but perturbed by the presence of the dc magnetic field. These modes are, therefore, called the modified waveguide modes. In the case of an open ferrite column, they are called the "modified dielectric modes" [14]. Since these modes are not predicted by the magnetostatic approximation, they are also named the "dynamic modes," [11], [12], [15]. The modified waveguide modes are designated $TE_{nm}^{s_0}$ or $TM_{nm}^{s_0}$ according to whether their cutoff frequencies are determined by the TE or TM cutoff curves.

Since the TE cutoff frequencies take any values between zero and infinity, they determine the cutoff frequencies of all the categories of the modes. The TM cutoff frequencies in regions B and C are larger than Ω_c and those in region A are smaller than Ω_c. Therefore, the cutoff curves $\overline{TM}_{np}^{s_0}$ determine the cutoff frequencies of the surface-wave modes and the modified waveguide modes, and the cutoff curves $\overline{V}_{np}^{s_0}$ determine the cutoff frequencies of the volume modes. It is clear that the mode order m used in the dispersion curves $V_{nm}^{s_0}$ is not necessarily the same as p in the cutoff curves $\overline{V}_{np}^{s_0}$. For example, the cutoff frequencies of the $V_{\pm 1,1}^{0.1}$ modes in Fig. 4(b) are determined by the cutoff curve $\overline{TE}_{1,1}{}^{0.1}$ in Fig. 3(a) and those of the $V_{\pm 1,2}^{0.1}$ modes in Fig. 4(b) are determined by the cutoff curves $V_{\pm 1,1}^{0.1}$ in Fig. 3(b).

For a weak dc magnetic field ($\Omega_H = 0.5$), the volume modes are strictly backward waves when $s_0 = 0.1$. The surface-wave modes $S_1{}^{0.9}$ and $S_1{}^{0.5}$ exist but the $S_1{}^{0.1}$ and $S_1{}^{1.}$ modes do not exist. The cutoff frequencies of the $S_1{}^{0.9}$ and $S_1{}^{0.5}$ are determined by the cutoff curves $\overline{TM}_{1,1}{}^{0.9}$ and $\overline{TM}_{1,1}{}^{0.5}$, respectively, in Fig. 3(b). Therefore, the $TM_{-1,1}^{0.9}$ and $TM_{-1,1}^{0.5}$ in Fig. 6(a) should be paired with $S_1{}^{0.9}$ and $S_1{}^{0.5}$, respectively.

For a strong dc magnetic field ($\Omega_H = 1.7$), the surface-wave modes do not exist and all the lower order volume modes are forward waves in region IV. The cutoff frequencies of the $V_{\pm 1,1}^{1.}$, $V_{\pm 1,1}^{0.9}$, $V_{-1,1}^{0.5}$, $V_{1,2}{}^{0.5}$, $V_{\pm 1,1}^{0.1}$, and $V_{\pm 1,3}^{0.1}$ modes in Fig. 5(a) and (b) are now determined by the cutoff curves $\overline{TE}_{1,1}{}^{1.}$, $\overline{TE}_{1,1}{}^{0.9}$, $\overline{TE}_{1,1}{}^{0.5}$, $\overline{TE}_{1,1}{}^{0.1}$, and $TE_{1,2}{}^{0.1}$, respectively, in Fig. 3(a), and the cutoff frequencies of the $V_{\pm 1,2}^{1.}$, $V_{\pm 1,3}^{1.}$, $V_{\pm 1,2}^{0.9}$, $V_{1,1}{}^{0.5}$, $V_{-1,2}^{0.5}$, and $V_{\pm 1,2}^{0.1}$ modes in Fig. 5(a) and (b) are determined by the cutoff curves $\overline{V}_{\pm 1,1}^{1.}$, $\overline{V}_{\pm 1,2}^{1.}$, $\overline{V}_{\pm 1,1}^{0.9}$, $\overline{V}_{\pm 1,1}^{0.5}$, and $\overline{V}_{\pm 1,1}^{0.1}$, respectively, in Fig. 3(b). The clear transitions from the forward to the backward wave nature are observed near the line $u_2{}^2 = 0$ especially for the modes with $n = -1$.

To explain the existence of the surface-wave modes, Fig. 8 is included. In this figure, $\Omega_H = 0.1$, i.e., very weak dc magnetic fields, the surface-wave modes $S_1{}^{0.9}$, $S_1{}^{0.5}$, and $S_1{}^{0.1}$ exist. As seen in Fig. 3(a) and (b), the $S_1{}^{0.9}$, $S_1{}^{0.5}$, and $S_1{}^{0.1}$ modes have their cutoffs determined by the cutoff curves $\overline{TM}_{1,1}{}^{0.4}$, $\overline{TM}_{1,1}{}^{0.5}$, and $\overline{TE}_{1,1}{}^{0.1}$, which are the lowest cutoff frequencies among the TE and TM cutoffs for $\Omega_H = 0.1$ and $q = 0.5$. Of course, these lowest cutoffs are also above Ω_c. It is concluded that the existence of the surface-wave modes depend on Ω_H, q, and s_0. When these parameters are fixed, they can only exist if their cutoffs are the lowest ones among the TE and TM cutoffs and are greater than Ω_c. In fact, in Fig. 4(b), there is no surface-

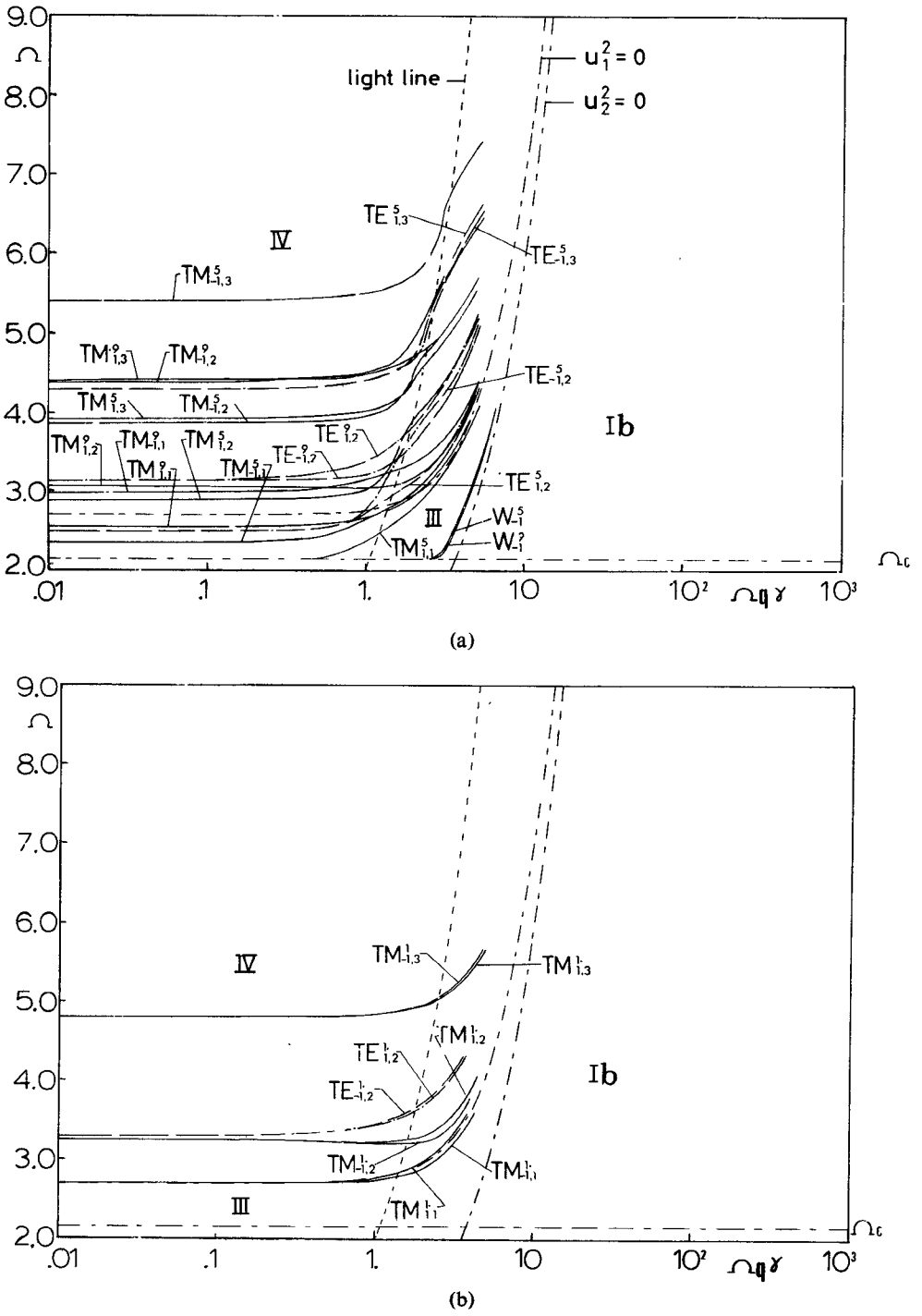

Fig. 7. (a) Modified waveguide modes for $n = \pm 1$, $q = 0.5$, $\Omega_H = 1.7$, $s_0 = 0.9, 0.5$, $\varepsilon_r = 10$. (b) Modified waveguide modes for $n = \pm 1$, $q = 0.5$, $\Omega_H = 1.7$, $s_0 = 1$, $\varepsilon_r = 10$.

wave mode for $s_0 = 0.1$ because the lowest cutoff among TE and TM cutoffs is the $\overline{\text{TE}}_{1,1}{}^{0.1}$ cutoff which is lower than Ω_c. The same arguments can be applied to explain the nonexistence of the surface-wave modes in Fig. 5(a) and (b). In the fully filled case, the $\text{TM}_{1,1}{}^{1}$ mode expected to be a surface-wave mode starts as a backward wave but changes to a forward wave and becomes a modified waveguide mode. The nonexistence of the surface-wave modes in the fully filled case can be explained by the fact that there is no air–ferrite interface to guide the surface waves.

By varying Ω_H, the behaviors of the surface-wave and volume modes change as follows: When Ω_H is small, the volume modes have a common cutoff frequency Ω_c [Fig. 3(b)]. For small q, all the cutoff frequencies of the TE modes are larger than Ω_c [Fig. 3(a)], which implies that the TE cutoff curves do not determine the cutoff frequencies of the volume modes. Consequently, for small Ω_H and q, the surface-wave and volume modes behave like those predicted by the magnetostatic analysis. As Ω_H increases, the multimode region II is shifted up, while the cutoff frequencies of

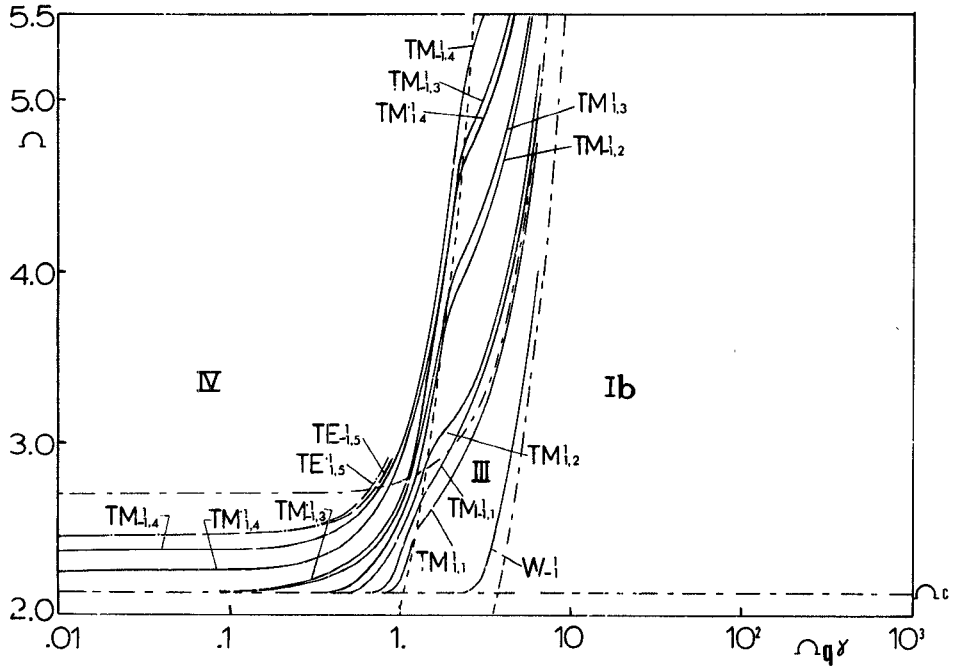

(c)

Fig. 7. (c) Modified waveguide modes for $n = \pm 1$, $q = 0.5$, $\Omega_H = 1.7$, $s_0 = 0.1$, $\varepsilon_r = 10$.

some lower order volume modes are now determined by the TE cutoff curves which are independent of Ω_H. As a result, the lower order volume modes start to propagate as the forward waves.

For the fully filled case, the surface-wave modes do not exist, while they exist in the partially filled case though their existence depends on Ω_H, s_0, and q. As noted in Section II-C, the $V^1_{-1,1}$ mode cannot be predicted in the magnetostatic approximation. However, there exists the $V^1_{-1,1}$ mode [see Figs. 4(b) and 5(b)] in the exact dispersion relation, which has a root of $u_1 a$ falling in the first interval of the quotient function [1]. Hence each pair of volume modes $V^1_{\pm 1,m}$ has values of $u_1 a$ falling in the same interval of the quotient function. In the partially filled case, each pair of volume modes has roots of $u_1 b$ falling in different intervals of the quotient function, i.e., there is no root in the first interval of the quotient function for $n = -1$.

For the higher order volume modes, the asymptotic dispersion equation (6) was used to obtain the dotted curves $V^{0.5}_{\pm 1,40}$ and $V^{0.9}_{\pm 1,50}$ in Figs. 4(a) and 5(a). As shown in Table II, the asymptotic results agree well with those computed from (A3) even for the third-order modes. Therefore, the asymptotic dispersion equations are very useful to obtain the dispersion curves of the higher order modes. Note that the agreement is better at $\Omega = 0.6$ than at $\Omega = 0.7$. This can be explained by the fact that, near cutoff ($\Omega = 0.7$), the dispersion equation (A3) depends on s_0, while the asymptotic equation (6) is independent of s_0, and that, near resonance ($\Omega = 0.6$), (A3) is almost independent of s_0.

The dispersion curves of the modified waveguide modes are shown in Fig. 6(a) and (c) for $\Omega_H = 0.5$ and in Fig. 7(a) and (c) for $\Omega_H = 1.7$. It is seen that these modes are not so strongly affected by the change of Ω_H. As Ω increases, the dispersion curves of the modified waveguide modes approach those of the corresponding modes existing in a waveguide partially or fully filled with a dielectric column. In particular, in the limit of $\Omega \to \infty$, all the dispersion curves are asymptotic to the line $\gamma = \varepsilon_r^{1/2}$ ($u_2^2 = 0$), which is the normalized phase velocity of electromagnetic waves in an infinite dielectric (ε_r) medium.

TABLE II
RESULTS OF EXACT ANALYSIS

	Computed Results		Asymptotic Results	
	Ω	$\Omega q \gamma$	Ω	$\Omega q \gamma$
$V^{.5}_{1,3}$	.7	7.88	.7	8.19
	.6	15.11	.6	15.34
$V^{.5}_{1,40}$	.7	128.31	.7	129.18
	.6	234.20	.6	234.2
$V^{.5}_{-1,3}$	.7	10.98	.7	11.46
	.6	20.70	.6	21.26
$V^{.5}_{-1,40}$	.7	132.41	.7	133.26
	.6	240.08	.6	240.13

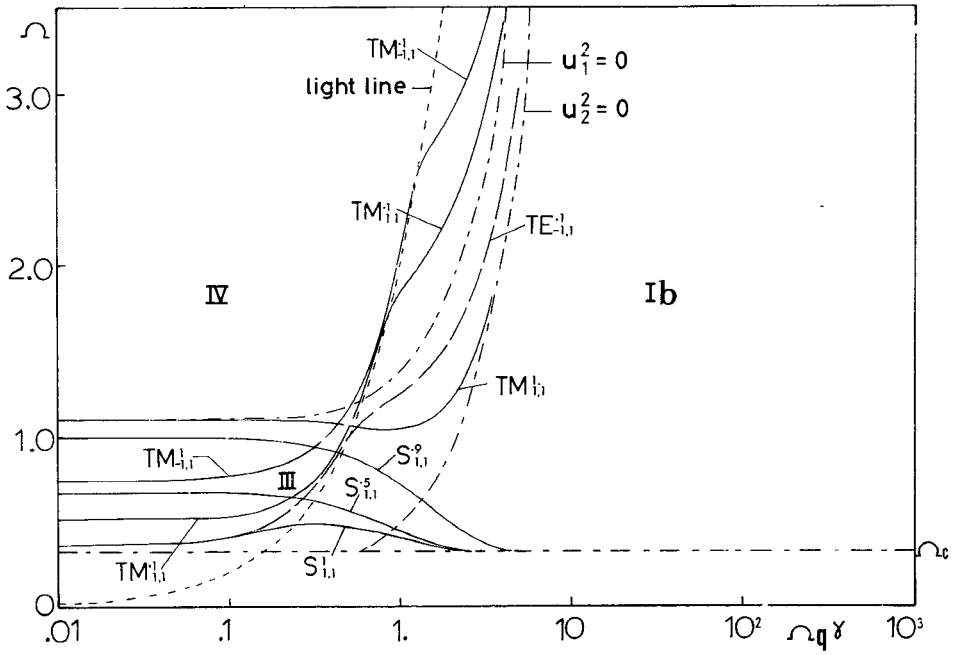

Fig. 8. Surface-wave modes and modified waveguide modes for $n = \pm 1$, $q = 0.5$, $\Omega_H = 0.1$, $s_0 = 1, 0.9, 0.5, 0.1$, $\varepsilon_r = 10$.

In Figs. 6(c) and 7(a) and (c), the lower order modes have their cutoffs at certain nonzero γ on the line $\Omega = \Omega_c$, where the group velocities of these modes at their cutoff points are zero. In Fig. 6(c), the $TM_{1,2}{}^{0.1}$ mode was so named since its cutoff frequency is determined by the cutoff curve $\overline{TM}_{1,2}{}^{0.1}$ in Fig. 3(b), and similarly for the higher order modes. The lower order modes are named $TM^{0.1}_{\pm 1,1}$ and $W_{-1}{}^{0.1}$. The pair of modes $TM^{0.1}_{\pm 1,1}$ are expected to have the corresponding cutoffs determined by $\overline{TM}^{0.1}_{\pm 1,1}$ curves, which terminate on the line $\Omega = \Omega_c$ in Fig. 3(b). The $W_{-1}{}^{0.1}$ mode behaves like the $TE^{0.1}_{-1,1}$ mode in Fig. 8. However, this mode cannot be predicted by the cutoff curves shown in Fig. 3(a) and (b). It is an unpaired waveguide mode. The same situation as in Fig. 6(c) occurs in Fig. 7(a) and (c), namely, the $TM_{1,1}{}^{0.5}$, $W_{-1}{}^{0.5}$, and $W_{-1}{}^{0.9}$ modes in Fig. 7(a), and the $TM^{0.1}_{\pm 1,3}$, $TM^{0.1}_{\pm 1,2}$, $TM^{0.1}_{\pm 1,1}$, and $W_{-1}{}^{0.1}$ modes in Fig. 7(c). As Ω_H increases, more cutoff curves merge into the line $\Omega = \Omega_c$ and, therefore, more modes start to propagate at nonzero γ.

IV. Comparisons Between Magnetostatic and Exact Results

Both magnetostatic and exact analyses yield the same asymptotic dispersion equations (6) and (7). This, therefore, confirms the validity of the magnetostatic analysis for large γ. However, the modified waveguide modes cannot be predicted by the magnetostatic analysis. The existence of the surface-wave modes depends on Ω_H, s_0, and q in the exact analysis, whereas they always exist for any values of Ω_H, s_0, and q. According to the exact analysis, the cutoff frequencies of the volume modes are not necessarily equal to Ω_c which is a common cutoff frequency for the magnetostatic volume modes, and the departures from Ω_c become larger as Ω_H increases and s_0 decreases. It is also noted that the magnetostatic dispersion equations (A1) and (A2) are independent of ε_r, causing a major error near cutoff.

For a relatively weak dc magnetic field, it is seen from Figs. 1(a) and (b) and 4(a) and (b) that the validity of the magnetostatic results for the volume modes is observed in region II, particularly for the higher order modes and for large s_0. For a relatively strong dc magnetic field, the validity of the magnetostatic results for the volume modes is restricted to the vicinity of the gyromagnetic resonance, as seen from Figs. 2(a) and (b) and 5(a) and (b). In the exact analysis, the lower order volume modes are forward waves in regions II and IV, while the magnetostatic volume modes are always backward waves. Moreover, the $V^{1}_{-1,1}$ mode could not be predicted in the magnetostatic approximation.

V. Conclusion

In general, the magnetostatic approximation is valid when γ is large. For a fixed value of γ, the validity depends on the strength of dc magnetic fields and the ratio of radii s_0. The exact analysis gives a major correction to the magnetostatic results in the fast-wave region, e.g., the modified waveguide modes, the forward nature of the volume modes, and the departure of their cutoff frequencies from Ω_c. The surface-wave modes always exist in the magnetostatic approximation. However, in the exact analysis they can only exist when Ω_H, q, and s_0 are such that the lowest cutoff frequency among TE and TM cutoffs is above Ω_c and they do not exist in the fully filled case. By varying s_0 and Ω_H, the fully filled waveguide, the ferrite column in free space, the uniaxial ferrite waveguide, and the isotropic ferrite waveguide can also be recovered. According to the physical characteristics of the various modes, they have been classified into the volume modes ${}^{\Omega_H}_{q}V^{s_0}_{n,m}$, the surface-wave modes ${}^{\Omega_H}_{q}S^{s_0}_{n}$, and the modified waveguide modes ${}^{\Omega_H}_{q}TE^{s_0}_{n,m}$ and ${}^{\Omega_H}_{q}TM^{s_0}_{n,m}$.

Since the dipolar modes are considered, the $n = 1$ and $n = -1$ modes have different phase velocities. Hence Faraday rotation exists. The angle of the Faraday rotation varies for different types of modes. Near the gyro-resonance frequency, this angle is found to be largest. Thus our results can have potential applications in gyrators, isolators, circulators, and particularly phase shifters [10], [13], [17].

The group velocity of the volume modes in the vicinity of the gyro-resonance is very small compared with the velocity of light. This low group velocity can reduce the length of a microsecond delay line from thousands of meters to a few centimeters [4], [18], [19].

Appendix I

Magnetostatic Dispersion Relations

$$\mu_1 \frac{J_n'(ub)}{J_n(ub)} - \mu_2 \frac{n}{b} = \frac{I_n'(kb)K_n'(ka) - I_n'(ka)K_n'(kb)}{I_n(kb)K_n'(ka) - I_n'(ka)K_n(kb)} \tag{A1}$$

$$\mu^2 = -\frac{k^2}{\mu_1}. \tag{A2}$$

Appendix II

Exact Dispersion Relations

$$\frac{f_\phi(u_1)}{f_r(u_1)} = \frac{f_\phi(u_2)}{f_r(u_2)} \tag{A3}$$

$$u_{1,2}^2 = k_0^2 \left\{ \frac{\varepsilon_r(1 + 2\Omega_H) + (\varepsilon_r - \gamma^2)(2\Omega_H^2 + \Omega_H - 2\Omega^2)}{2(\Omega_H^2 + \Omega_H - \Omega^2)} \right\} \pm \frac{[\{\Omega_H^2\gamma^2 - \varepsilon_r(\Omega_H^2 + \Omega_H - 2\Omega^2)\}^2 + 4\varepsilon_r^2\Omega^2(\Omega_H^2 + \Omega_H - \Omega^2)]^{1/2}}{2\Omega_H(\Omega_H^2 + \Omega_H - \Omega^2)} \tag{A4}$$

$$f_\phi(u_i) = \Delta^{-1} \left[\frac{n}{b} \{\varepsilon_r(\mu_1 \mp \mu_2) - \gamma^2\}\{y(\eta_i) \pm \varepsilon_r\} - \varepsilon_r\{\varepsilon_r\mu_1 - \gamma^2 - \mu_2 y(\eta_i)\} \left\{ \frac{\pm u_i J_{n\mp1}(u_i b)}{J_n(u_i b)} \right\} \right] - \left\{ G_n(u_0, b) - \frac{n}{b} y(\eta_i) \right\} (1 - \gamma^2)^{-1} \tag{A5}$$

$$f_r(u_i) = \frac{n}{b} \left\{ \frac{[\varepsilon_r(\mu_1^2 - \mu_2^2) - \gamma^2(\mu_1 \pm \mu_2)]}{\Delta} \cdot [-\varepsilon_r \mp y(\eta_i)] - \frac{1}{1 - \gamma^2} \right\} + \left\{ \frac{-\varepsilon_r\gamma^2\mu_2 + [\varepsilon_r(\mu_1^2 - \mu_2^2) - \gamma^2\mu_1]y(\eta_i)}{\Delta} \right\} \cdot \left\{ \frac{\pm u_i J_{n\mp1}(u_i b)}{J_n(u_i b)} \right\} + \frac{y(\eta_i)}{1 - \gamma^2} H_n(\mu_0, b) \tag{A6}$$

$$u_0 = k_0(1 - \gamma^2) \qquad u_i = k_0\eta_i, \qquad i = 1,2$$

$$y(\eta_i) = \frac{\eta_i^2(\varepsilon_r\mu_1 - \gamma^2) + \Delta}{\mu_2\eta_i^2}, \qquad \Delta = (\varepsilon_r\mu_2)^2 - (\varepsilon_r\mu_1 - \gamma^2)^2 \tag{A7}$$

$$H_n(\mu_0, b) = \frac{J_n'(\mu_0 b)N_n'(\mu_0 a) - J_n'(\mu_0 a)N_n'(\mu_0 b)}{J_n(\mu_0 b)N_n'(\mu_0 a) - J_n'(\mu_0 a)N_n(\mu_0 b)} \tag{A8}$$

$$G_n(\mu_0, b) = \frac{J_n'(\mu_0 b)N_n(\mu_0 a) - J_n(\mu_0 a)N_n'(\mu_0 b)}{J_n(\mu_0 b)N_n(\mu_0 a) - J_n(\mu_0 a)N_n(\mu_0 b)}. \tag{A9}$$

Appendix III

At cutoff frequencies, the modes are no longer hybrid in nature but are pure TE and TM. The dispersion relations are as follows.

Transverse Electric Modes

$$\frac{J_n'(u_2 b)}{\varepsilon_r J_n(u_2 b)} = \frac{J_n'(k_0 b)N_n'(k_0 a) - J_n'(k_0 a)N_n'(k_0 b)}{J_n(k_0 b)N_n'(k_0 a) - J_n'(k_0 a)N_n(k_0 b)}. \tag{A10}$$

$$u_2^2 = k_0^2\varepsilon_r. \tag{A11}$$

Transverse Magnetic Modes

$$\frac{1}{\mu_1^2 - \mu_2^2} \left[\mu_1 \frac{J_n'(u_1 b)}{J_n(u_1 b)} + \mu_2 \frac{n}{b} \right] = \frac{J_n'(k_0 b)N_n(k_0 a) - J_n(k_0 a)N_n'(k_0 b)}{J_n(k_0 b)N_n(k_0 a) - J_n(k_0 a)N_n(k_0 b)} \tag{A12}$$

$$u_1^2 = k_0^2 \left[\frac{\varepsilon_r[(\Omega_H + 1)^2 - \Omega^2]}{\Omega_H^2 + \Omega_H - \Omega^2} \right]. \tag{A13}$$

References

[1] G. L. Yip and S. Le-Ngoc, "Dispersion characteristics of the dipolar modes in a wave guide partially filled with a magneto-plasma column," *Canadian J. Phys.*, vol. 53, pp. 1163–1178, June 1975.

[2] A. W. Trivelpiece, A. Ignatius, and P. C. Holscher, "Backward waves in longitudinally magnetized ferrite rods," *J. Appl. Phys.*, vol. 32, pp. 259–267, Feb. 1961.

[3] R. I. Joseph and E. Schlömann, "Theory of magnetostatic modes in long, axially magnetized cylinders," *J. Appl. Phys.*, vol. 32, pp. 1001–1005, June 1961.

[4] M. Bini, L. Millanta, N. Rubino, and I. Kaufman, "Magnetostatic waves in axially magnetized cylinders: Experimental dispersion curves," *Il Nuovo Cimento*, vol. 47, pp. 281–293, Feb. 1967.

[5] F. A. Olson, E. K. Kirchner, K. B. Mehta, F. J. Peternell, and B. C. Morley, "Propagation of magnetostatic surface waves in YIG rods," *J. Appl. Phys.*, vol. 38, pp. 1218–1220, Mar. 1967.

[6] M. Masuda, N. S. Chang, and Y. Matsuo, "Azimuthally dependent magnetostatic modes in the cylindrical ferrites," *IEEE Trans. Microwave Theory Tech.*, vol. MTT-19, pp. 834–836, Oct. 1971.

[7] M. Kales, "Modes in wave guides containing ferrites," *J. Appl. Phys.*, vol. 24, pp. 604–608, May 1953.

[8] H. Suhl and L. R. Walker, "Topics in guided wave propagation through gyromagnetic media, Part I," *Bell Syst. Tech. J.*, vol. 33, pp. 579–659, May 1974.

[9] J. E. Tompkins, "Energy distribution in partially ferrite-filled waveguides," *J. Appl. Phys.*, vol. 29, pp. 399–340, Mar. 1958.

[10] A. M. Duputz and A. C. Priou, "Computer analysis of microwave propagation in a ferrite loaded circular waveguide—Optimization of phase-shifter longitudinal field sections," *IEEE Trans. Microwave Theory Tech.*, vol. MTT-22, pp. 601–613, June 1974.

[11] F. W. Schott, T. F. Tao, and R. A. Freibrun, "Electromagnetic waves in longitudinally magnetized ferrite rods," *J. Appl. Phys.*, vol. 38, pp. 3015–3022, June 1967.

[12] T. F. Tao, J. W. Tully, and F. W. Schott, "Dynamic mode surface waves on magnetized YIG ferrite rods," *Appl. Phys. Lett.*, vol. 14, pp. 106–108, Feb. 1969.

[13] R. E. Collin, *Foundations for Microwave Engineering*. New York: McGraw-Hill, 1966, p. 286.

[14] P. De Santis and G. Franceschett, "Dynamic modes in open gyromagnetic waveguides," *J. Appl. Phys.*, vol. 43, pp. 2012–2014, Apr. 1972.

[15] F. W. Schott and T. F. Tao, "On the classification of electromagnetic waves in ferrite rods," *IEEE Trans. Microwave Theory Tech.*, vol. MTT-16, pp. 959–961, Nov. 1968.

[16] P. De Santis and G. Franceschett, "Hybrid-frequency cutoffs in gyrotropic waveguides," *IEEE Trans. Microwave Theory Tech.*, vol. MTT-20, pp. 237–238, Mar. 1972.

[17] W. E. Hord, F. J. Rosenbaum, and J. A. Bennet, "Theory and operation of a reciprocal Faraday-rotation phase shifter," *IEEE Trans. Microwave Theory Tech.*, vol. MTT-20, pp. 112–119, Feb. 1972.

[18] F. A. Olson and J. R. Yager, "Microwave delay techniques using YIG," *IEEE Trans. Microwave Theory Tech.*, vol. MTT-13, pp. 63–69, Jan. 1965.

[19] V. Bini, L. Millanta, N. Rubino, and V. Tognetti, "Time-delay limits set by dispersion in magnetostatic delay lines," *IEEE Trans. Microwave Theory Tech.*, vol. MTT-20, pp. 771–773, Nov. 1972.